Contents lists available at ScienceDirect

NeuroImage: Clinical

journal homepage: www.elsevier.com/locate/ynicl

NeuroImage: CLINICAL

CrossMark

Defining the anterior nucleus of the thalamus (ANT) as a deep brain stimulation target in refractory epilepsy: Delineation using 3 T MRI and intraoperative microelectrode recording

T. Möttönen[a,*], J. Katisko[b], J. Haapasalo[a], T. Tähtinen[a], T. Kiekara[c], V. Kähärä[c], J. Peltola[a], J. Öhman[a], K. Lehtimäki[a]

[a]Department of Neurosciences and Rehabilitation, Tampere University Hospital, P.O. Box 2000, Tampere 33521, Finland
[b]Department of Neurosurgery, Oulu University Hospital, P.O. Box 21, Oulu 90029, Finland
[c]Medical Imaging Centre, Tampere University Hospital, P.O. Box 2000, Tampere 33521, Finland

ARTICLE INFO

ABSTRACT

Background: Deep brain stimulation (DBS) is a minimally invasive and reversible method to treat an increasing number of neurological and psychiatric disorders, including epilepsy. Targeting poorly defined deep structures is based in large degree on stereotactic atlas information, which may be a major source of inconsistent treatment effects.
Aim of the study: In the present study, we aimed to study whether a recently approved target for epilepsy (anterior nucleus of thalamus, ANT) is visualized in clinically established 3 T MRI and whether ANT is delineated using intraoperative microelectrode recording (MER). We have especially focused on individual variation in the location of ANT in stereotactic space. We also aimed to demonstrate the role of individual variation in interpretation of MER data by projecting samples onto AC–PC (anterior and posterior commissure) and ANT-normalized coordinate systems.
Methods: Detailed analysis of ANT delineations in 3 T MRI short tau inversion recovery (STIR) images from eight patients undergoing DBS for refractory epilepsy was performed. Coronal and sagittal cross-sectional models of ANT were plotted in the AC–PC coordinate system to study individual variation. A total of 186 MER samples collected from 10 DBS trajectories and 5 patients were analyzed, and the location of each sample was calculated and corrected accordingly to the location of the final DBS electrode and projected to the AC–PC or coordinate system normalized to ANT.
Results: Most of the key structures in the anatomic atlas around ANT (mammillothalamic tract and external medullary lamina) were identified in STIR images allowing visual delineation of ANT. We observed a high degree of anatomical variation in the location of ANT, and the cross-sectional areas overlapped by study patients decreased in a linear fashion with an increasing number of patients. MER information from 10 individual trajectories correlated with STIR signal characteristics by demonstrating a spike-negative zone, presumably white matter layer, at the lateral aspect of ANT in ANT-normalized coordinate system as predicted by STIR images. However, MER information projected to the AC–PC coordinate system was not able to delineate ANT.
Conclusions: ANT is delineated in 3 T MRI by visualization of a thin white matter lamina between ANT and other nuclear groups that lack spiking activity. Direct targeting in the anterior thalamic area is superior to indirect targeting due to extensive individual variation in the location of ANT. Without detailed imaging information, however, a single trajectory MER has little localizing value.

1. Introduction

Deep brain stimulation (DBS) is a widely used minimally invasive and reversible method to treat various neurological and psychiatric disorders by stimulating deeply located structures in the brain, and its use is estimated to expand in the future. Implantation of electrodes into a target not visible in current imaging methods can be performed using stereotactic principles, where the target structure location is

first defined in the atlas brain relative to common visible anatomic landmarks such as the anterior commissure (AC) and posterior commissure (PC), and the same coordinates relative to the AC–PC line are used to access the non-visible target in the patient brain (indirect targeting method). Due to the development of imaging techniques, indirect targeting has mostly been replaced by direct targeting based on visualization of the desired target structure in the patient's images. In theory, the use of indirect (AC–PC based) targeting is limited due to potential anatomical variation in the location of the target structure between individuals and stereotactic atlas information, whereas the direct targeting method is limited due to a lack of adequate target specific MRI imaging methods. Advances in sophisticated imaging modalities have led to the replacement of indirect targeting with direct targeting in most indications. However, due to a lack of direct imaging methods, indirect targeting is still widely used in DBS of the anterior nucleus of the thalamus (ANT).

DBS of the anterior nucleus of the thalamus (ANT) has been suggested as a treatment option in refractory focal epilepsy by a large-scale randomized controlled trial (Fisher et al., 2010) and several open-label pilot studies (Hodaie at al., 2002; Kerrigan et al., 2004; Lee et al., 2012). However, ANT is poorly identified in currently used MRI techniques adopted from movement disorder surgery. A recent report suggests that ANT boundaries are identified in 3 T MRI T1 images (Buentjen et al., 2014), most likely due to visualization of the white matter laminae around the ANT. Moreover, visualization of the white matter laminae in the thalamus by 3 T MRI short tau inversion recovery (STIR) images has been suggested (Yamada et al., 2010).

ANT, with its extensive connections to the subicular cortex, cingulum, mammillary bodies and retrosplenial cortex, is an integral part of the hippocampal system for episodic memory, and is also thought to be involved in executive and emotional functions. Animal studies have pointed to ANT having a role in the generalization of focal cortical seizures. (Child and Benarroch, 2013) Animal models have also proven that high-frequency stimulation of ANT can inhibit induced ictal activity in the hippocampus (Stypulkowski et al., 2011).

The aim of the present study is to study the delineations of ANT using 3 T MRI STIR sequence and to provide information about the size and shape of ANT as well as to measure the degree of anatomical variation/overlap in the location of ANT in an AC–PC based coordinate system between individuals. Secondly, we aimed to study whether ANT can be delineated using microelectrode recording (MER), a method widely used in movement disorder surgery, which can be regarded as an alternative electrophysiological imaging modality differentiating white and gray matter based on their firing properties. Finally, we aimed to demonstrate the role of individual variation in interpretation of MER data by comparing the MER data projected to an AC–PC and ANT-normalized coordinate system.

2. Materials and methods

2.1. Imaging

Eight patients with refractory epilepsy underwent magnetic resonance imaging for planning of surgery. The sequences obtained included isotropic 3D-T1W with 0.9 mm slices for multi-plane reconstruction, axial T2W, and STIR in all three imaging planes. All images were obtained using a 3 T scanner (MAGNETOM Trio 3 T, Siemens Healthcare Sector, Erlangen, Germany) with a 12-channel head matrix coil. The STIR sequence used was a 2D turbo inversion recovery sequence with a short inversion time (TR/TE/TI = 8300 ms/22 ms/120 ms: acquisition time 7.05 min), with a slice thickness/gap of 2.0/0.2 mm, matrix size 256 × 256 and field of view of 235 mm. Intravenous contrast was used for the 3D-T1W images.

2.2. Delineation procedure of the ANT in STIR images

All images were analyzed using Leksell SurgiPlan software (Elekta AB, Stockholm, Sweden). At first, midpoints of the anterior commissure–posterior commissure (AC–PC) line were defined in the 3D-T1-weighted images. Next, a co-registration of STIR and 3D-T1 contrast images was performed. Stereotactic coordinates relative to the mid-commissural point (MCP) of the points along the delineated borders of the ANT in the coronal and sagittal orientations were collected. Thereafter, a cross-sectional model of ANT was calculated in the sagittal and coronal orientations and plotted onto an AC–PC based coordinate system. These delineations were also used for measurements of length, height, width and cross-sectional area of the ANT in each thalamus (Table 1). To study anatomical overlap between individuals in stereotactic space, each anatomical model was taken into a common AC–PC based coordinate system. The degree of anatomical overlap was expressed as overlapping area (mm^2, Fig. 3) as a function of the number of patients. Targeting for implantation was performed by using AC–PC based coordinates as a starting point and adjusting the target directly from the images to account for anatomical variations.

2.3. Microelectrode recording

Imaging results suggest that ANT is delineated by myelin-rich white matter lamina. To test this hypothesis, a total of 186 intraoperative microelectrode recording samples recorded from 10 trajectories in five patients were analyzed with respect to the presence of spikes. Single-track MER data were collected from five patients bilaterally. Five trajectories were paraventricular (bilateral in two cases) and five were transventricular. We used high impedance MicroMacro electrode and ISIS MER System by Inomed Medizintechnik GmbH, Emmendingen, Germany. Surgery and thus also the microelectrode recordings were performed under general anesthesia except in one case.

Recordings were obtained with 1-mm intervals starting from 10 mm before the calculated target, with 0.5-mm intervals starting from 5 mm before the target point, and extending to 3–5 mm beyond the target. Representative 2-s samples were chosen for every recording depth. The spike frequency was calculated for each sample (the number of > 25 μV spikes/2s). In transventricular trajectories, the most superior samples, clearly representing the cerebrospinal fluid, were excluded. In paraventricular trajectories, extending the measurement beyond the target point was mostly dismissed to avoid entering the third ventricle or the internal cerebral vein.

Each depth along a planned trajectory was considered to represent a point in stereotactic space. The location of each recorded sample was calculated relative to MCP and corrected according to the location of the final DBS electrode in the postoperative CT-preoperative MRI fusion images to account for surgical error. Samples were analyzed on the basis of whether or not they had spikes typical of thalamic nuclei. A sample lacking spiking activity was hypothesized to represent white matter. Due to extensive anatomical variation in the location of ANT in the AC–PC based coordinates, it was expected that the samples from different individuals might not be sufficient to test whether ANT is delineated using MER.

To overcome anatomical variation we decided to use boundaries of ANT in STIR images as a frame of another coordinate system instead of AC–PC. In this ANT-normalized coordinate system the medial and inferior borders of ANT in a coronal STIR image through the mammillothalamic tract was defined as the zero level, and the lateral and superior borders of the ANT as 1 (Fig. 4C).

SPSS 17.0 was used to visualize variation in the ANT location as well as to demonstrate correlation between MER and imaging information.

Consent was obtained from the patients and the study was approved by the Ethical Review Board of Pirkanmaa Hospital District.

Table 1
Morphological features of ANT in study patients.

| Patient	Length (mm)		Height (mm)		Width (mm)		Cross-sectional area Coronal (mm²)		Cross-sectional area Sagittal (mm²)	
	Left	Right	Left	Right	Left	Right	Left	Right	Left	Right
1	10.8	13.0	4.1	3.6	5.5	4.8	11.3	14.5	37.5	35.8
2	10.0	11.5	3.5	4.0	5.3	5.6	13.3	12.5	29.3	32.5
3	7.5	7.8	2.3	3.9	5.3	5.8	6.3	12.3	12.8	21.3
4	10.0	11.7	3.6	4.5	5.7	5.6	19.3	16.0	28.8	37.0
5	13.3	12.8	3.5	3.5	5.4	5.6	19.8	13.3	40.3	37.3
6	12.0	9.0	4.9	3.6	5.0	5.1	16.5	17.8	42.0	24.0
7	11.3	10.5	5.4	4.2	5.6	5.6	14.0	15.0	38.3	27.0
8	9.0	10.3	3.5	3.8	6.1	5.1	12.5	10.8	22.8	30.8
Mean	10.0	10.1	3.8	3.9	5.5	5.4	14.1	14.0	31.5	30.7
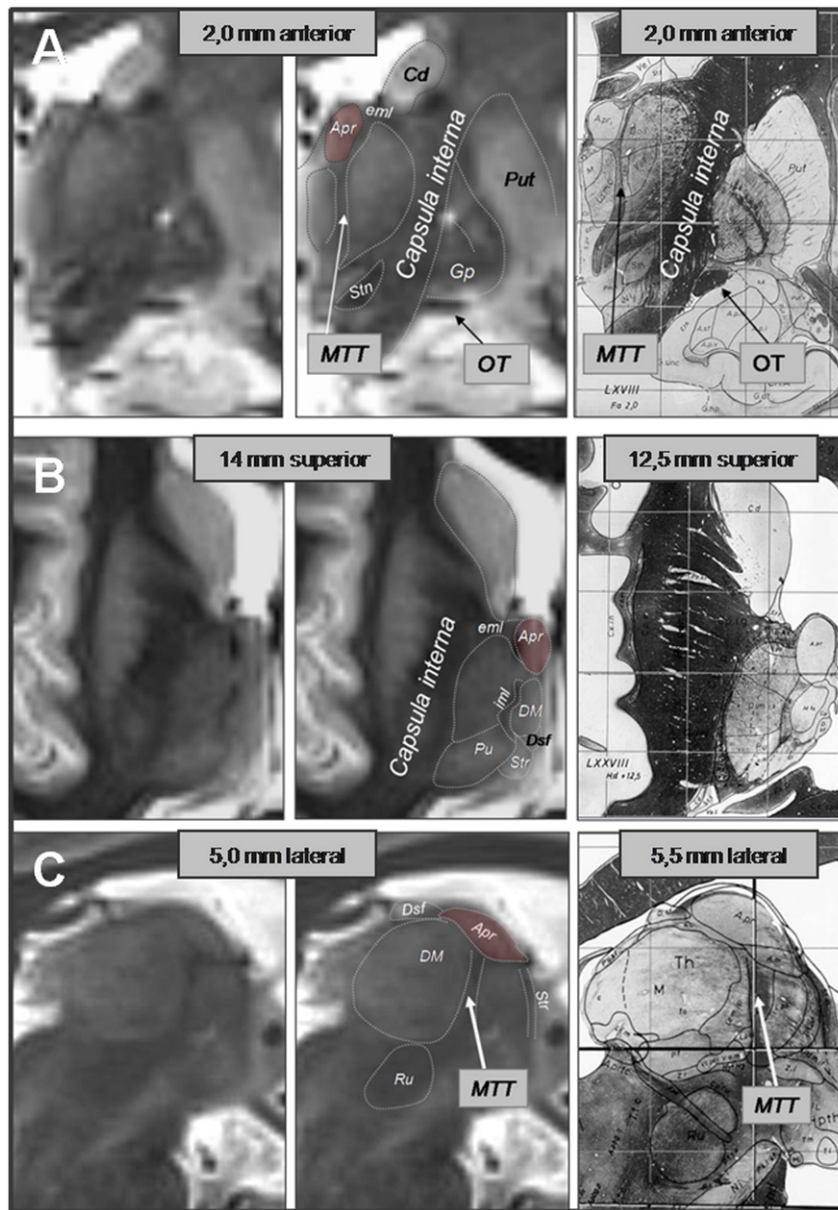
Fig. 1. Comparison between Schaltenbrand atlas and 3 T MRI STIR images. Atlas images reproduced with permission from Thieme Medical Publishers, Inc. Abbreviations: Apr, anterior principal nucleus; Cd, nucleus caudatus; DM, dorsomedial nucleus of thalamus; DSF, dorsal superficial nucleus; eml, external medullary lamina; Gp, Globus pallidum; iml, internal medullary lamina; MTT, mammillothalamic tract; OT, optic tract; Put, putamen; Pu, pulvinar; Ru, nucleus ruber; STN, subthalamic nucleus; Str, stria medullaris.

3. Results

3.1. 3 T STIR images and brain atlas

A detailed comparison of STIR images (patient 4 is shown due to most demonstrative anatomy) and the atlas by Schaltenbrand and Wahren (1998) in axial, sagittal and coronal orientations is presented in Fig. 1. We found out that most of the key structures around ANT were in fact visualized in STIR images. The most important and most clearly visualized structure was the mammillothalamic tract that was clearly visualized in the coronal and axial images and occasionally also in the sagittal images. Coronal STIR images also visualize a thin area of low signal intensity hypothesized to represent a white matter lamina between ANT and the ventral anterior nucleus (VA). The infero-medial aspect of the ANT was less clearly delineated similarly to the stereotactic atlases.

In the axial images, ANT was most clearly delineated in its anterior and lateral aspect, where ANT was delineated by presumably white matter structures having low signal intensity in STIR images correlating with external medullary lamina in anatomic atlas (Mai et al., 2007). In some patients, the internal medullary lamina separating the dorsomedial thalamus and lateral nuclear group was visible in the axial images (Fig. 1). Sagittal images occasionally demonstrated (depending on the level of the image slice in a particular patient) mammillothalamic tract and internal medullary lamina inferior to ANT. Distinct dorsal superficial (DSF) subnucleus of the ANT was visible in a subgroup of patients in sagittal images. Coronal STIR images showed the dorsal superficial nucleus as a more flat nucleus located posterior, slightly more superior and lateral compared to the anterior principal (Apr) and anteromedialis subnuclei (AM, not shown). Overall, we observed a high degree of correlation between STIR images and available anatomical atlases, in the sense that structures in atlases were readily identifiable from the images.

3.2. Morphology of ANT

Morphological measurements from each cross-sectional model of ANT based on delineation in 3 T MRI STIR images are presented in Table 1. The mean length of ANT (along the anterior–posterior axis of ANT) in sagittal orientation was ≈10 mm. The mean width of ANT in coronal images (perpendicular to the superior–inferior axis of ANT) was ≈5.5 mm and the mean maximal height of ANT in sagittal images (along the superior–inferior axis of ANT) was ≈4 mm (Table 1). The cross-sectional area of ANT in coronal images was ≈14 mm^2 and the cross-sectional area in sagittal images was ≈30 mm^2. Fig. 2 also demonstrates a high degree of variation in the shape of ANT.

3.3. The location of ANT in the AC–PC-based coordinate system

To study the variation in the location of ANT between individuals, each anatomical model was plotted onto the same AC–PC based coordinate system relative to MCP (Fig. 2). Our analyses revealed a high degree of anatomical variation in the location of ANT between individuals as expected.

The number of overlapping cross-sectional models corresponding to individual patients in the AC–PC based coordinate system is presented in Fig. 2. The overlapping cross-sectional areas declined in a linear fashion as function of number of the patients (Fig. 3). Noteworthily, no area observed in this patient group was overlapped by all eight patients in coronal or sagittal orientations. Compared to the Schaltenbrand atlas, ANT was consistently located more superiorly, anteriorly and laterally (Fig. 2).

3.4. Delineation of ANT using microelectrode recording

The spike frequency in MER samples in the AC–PC based coordinate system (Fig. 4A) and ANT-normalized (Fig. 4B) is demonstrated in Fig. 4. We were able to demonstrate two anatomically distinct groups of spikes
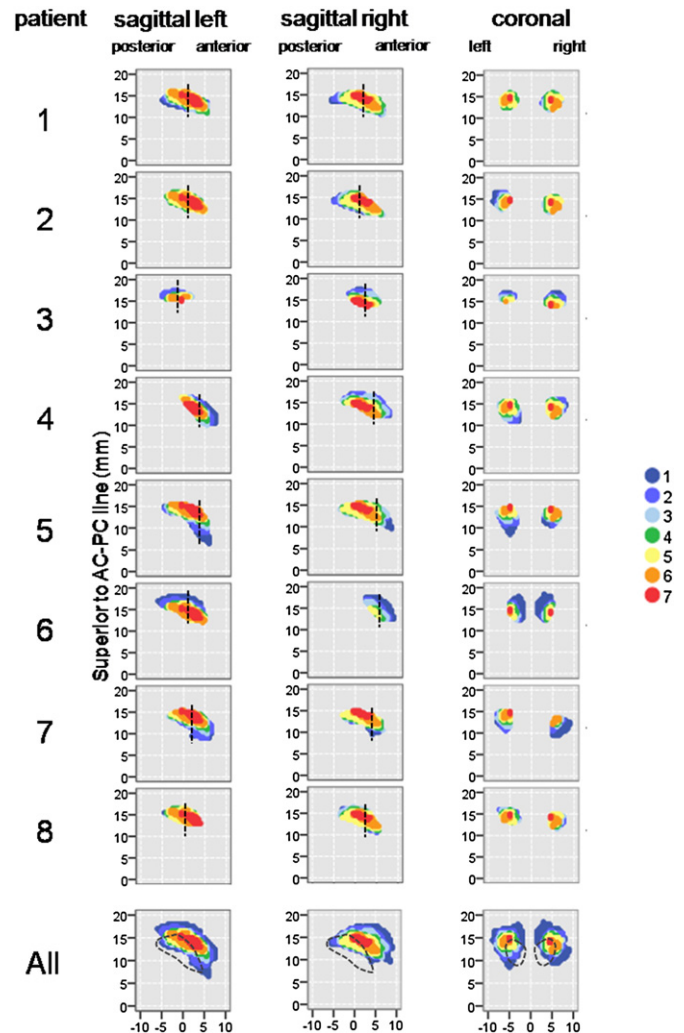

Fig. 2. Anatomical variation and cross-sectional overlap between patients. The relationship between each individual anatomical model and the whole patient group and anatomic atlas is presented. Each individual ANT model (one to eight) is demonstrated in the AC–PC coordinate system. The colors represent the degree of overlap (from 1–7) with the whole patient group, thus illustrating the deviation of a particular patient from the whole patient group. The vertical dashed line in sagittal ANT models represents the level of the coronal ANT model in y-axis. Since the coronal models were delineated from STIR image slices visualizing the mammillothalamic tract, the line also illustrates the anatomical relationship between the junction of mammillothalamic tract and ANT in individual patients. In the lower part of the image, the degree of overlap is presented in the whole patient group together with delineation of ANT in the Schaltenbrand atlas (dashed outlines). The data demonstrate that ANT was located more laterally, superiorly and anteriorly in 3 T MRI in this patient group compared to the anatomical atlas.

using the ANT-normalized coordinate system (Fig. 4C). When projected to the anatomical atlas normalized to ANT, the first group is located in an area correlating with ANT (red) and the second is correlated with VA (blue) (Fig. 4B). The projection of the same samples into the AC–PC based coordinate system relative to MCP shows that samples originating from different nuclei overlapped to a significant degree (Fig. 4A).

To further test the hypothesis that ANT is surrounded by myelin-rich white matter lamina, we carried out a spatial density analysis of MER samples which also included samples without spiking activity. The spatial density of the samples with spikes (ANT spikes or VA spikes based on frequency analysis) and the samples without spikes is presented in the AC–PC based (Fig. 5A) and ANT-normalized coordinate systems (Fig. 5B). The most superior samples from transventricular trajectories ($n = 5$) with fluid characteristics in MER were regarded as samples from the cerebrospinal fluid and were presented as a separate group. Two spatially distinct groups of spikes were identified similarly to the
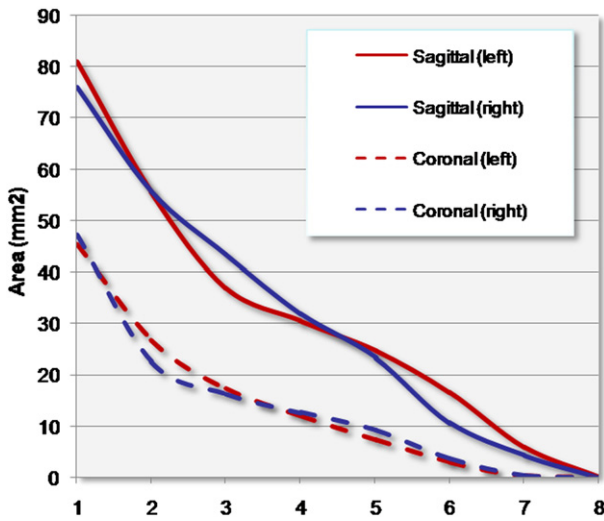
Fig. 3. The cross-sectional area overlapped by study subjects in sagittal and coronal orientations.

spike frequency analysis in ANT-normalized coordinate system. Importantly, the spike negative samples were most frequent in an area between these two groups of spikes in ANT-normalized coordinate system. Instead, when the location of the same samples was expressed relative to MCP using the AC–PC coordinate system the spatial density of the different sample groups peaked in a relatively small area without clearly separated density peaks from different origins of samples as suggested by ANT-normalized coordinate system.

A correlation between localization of the spikes and STIR image signal characteristics is demonstrated in Fig. 4C, where two groups of

spikes are evident in an area correlating with ANT and VA in STIR image, and lack of spikes in an area with low signal intensity consistent with white matter lamina.

4. Discussion

In the present study, we aimed to study the variation in the location of ANT and combine imaging information to the electrical properties of the anterior thalamic tissue. We were able to demonstrate that ANT is delineated using 3 T MRI STIR images visualizing white matter laminae around ANT. The clear need for direct visualization of ANT for clinical practice in treating refractory epilepsy with DBS was demonstrated by the high degree of interindividual variation and low degree of anatomical overlap in the location of ANT in the commonly used AC–PC coordinate system. Using visible boundaries of ANT in 3 T MRI STIR images as a frame for the coordinate system, it was possible to combine atlas/STIR images with MER samples showing spikes originating from ANT and VA. These samples were separated by samples lacking spiking activity, thus confirming our hypothesis based on signal characteristics in STIR imaging about white matter laminae around ANT.

The size and shape of ANT based on 3 T MRI imaging visually correlates with available atlas information (Mai et al., 2007; Schaltenbrand and Wahren, 1998). Atlas information suggests that the anterior part of the ANT (corresponding to the anterior principal (APr) and anterior medial (AM) subnuclei) is located inferiorly and medially while more posteriorly ANT runs slightly laterally and superiorly and has a more flat appearance (Mai et al., 2007). The length of the nucleus in our study was approximately 10 mm with a height of 5 mm and a width of 4 mm, which is comparable to atlas data (Mai et al., 2007; Schaltenbrand and Wahren, 1998). In most patients, the right ANT was located slightly more anteriorly compared to the left side. It should be noted that ANT was identifiable usually only in a few images from each patient (due to e.g. 2-mm slice thickness). It may be speculated
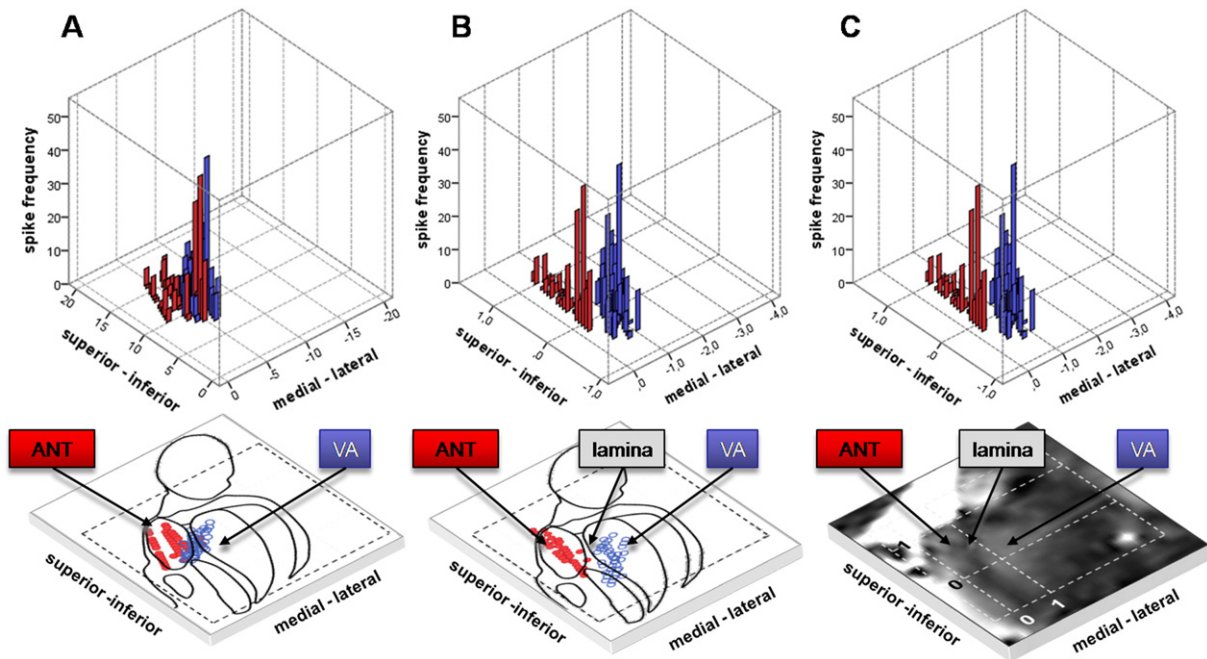

Fig. 4. Spike frequency data projected to the thalamus using AC–PC and ANT-normalized coordinate systems. The frequency of spikes in MER samples and the location of the sample projected to the AC–PC based coordinate system (A) and ANT-normalized coordinate system (B, C). Using ANT-normalized coordinate system two anatomically separate groups of spikes were identified (B). The projection of spikes onto the atlas of Mai (plate 12 mm posterior to AC) revealed high a correlation between the medial/superior group of spikes (red) with the boundaries of ANT and a lateral/inferior group of spikes with the boundaries of ventral anterior nucleus (VA) (blue). Projection of the samples to the AC–PC based coordinate system (A) demonstrates that the groups of spikes are spatially overlapped to a significant degree without clear, recognizable projection to any specific nucleus of the thalamus. Projection of the spikes onto STIR image (C) demonstrates a high degree of correlation between STIR signal characteristics and MER data, where spikes are present in ANT and VA but presumed white matter lamina lacks spiking activity.
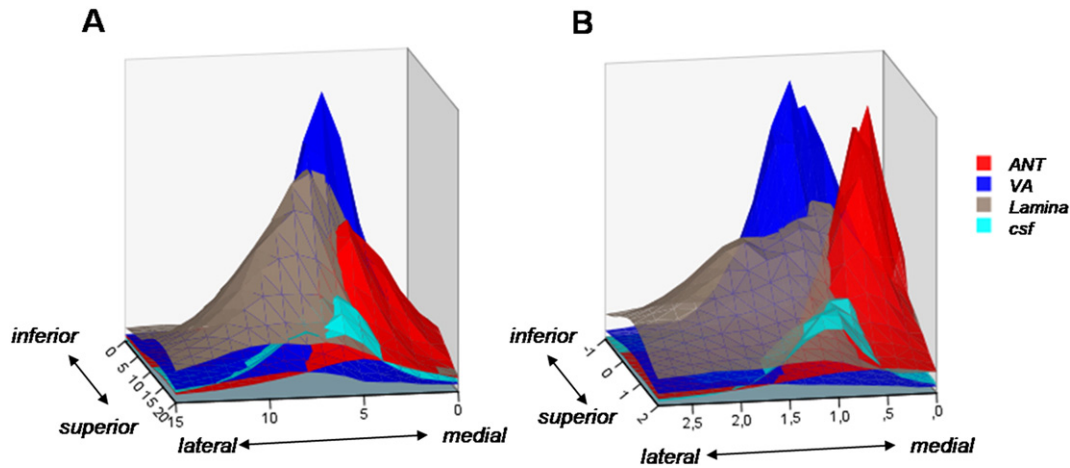
Fig. 5. The spatial relationship between samples with spikes and no spikes in the ANT-STIR based coordinate system (A) and AC–PC based coordinate system (B). The spatial density of samples with spikes correlating with ANT (red) and VA (blue) in the spike frequency analysis is presented together with the density of spike-negative samples. The most superior MER samples from patients with transventricular trajectories (and MER signal without any neural activity) were regarded as samples representing the CSF, and are presented separately (light blue). Spike-negative samples with somewhat higher background activity or minor spiking activity are hypothesized to represent white matter laminae (gray). In the ANT-normalized coordinate system, two groups of spikes suggested to originate from ANT (red) and VA (blue) are separated by spike-negative samples representing most likely the white matter lamina (B). Thus, the distribution of spikes and spike-negative samples from different individuals in ANT-normalized coordinate system shows a correlation with anatomic atlas information. Using the same color-coding of the samples in the AC–PC coordinate system (A) shows the peaking of sample densities from different sources (ANT/VA/lamina) in a relatively small area with a poor spatial resolution.

that visualization of the nucleus using MRI with the aforementioned somewhat oblique appearance, the level of MRI image relative to the nucleus may have a relatively large impact on the observed morphology and cross-sectional area of the nucleus. However, our current imaging method does not allow for multiplanar visualization of the ANT within a reasonable scanning time. Isotropic 3D-STIR might prove helpful, and we intend to test it.

Anatomical variation of the anterior nucleus has been previously described in an anatomical study (Van Buren and Borke, 1972). Our study confirms and extends this finding using modern imaging techniques. Visualization of ANT has been recently demonstrated in 3 T T1 images using a tight-fitting 32-channel head coil and 2 averages (Buentjen et al., 2014), allowing demarcation and direct targeting of this nucleus. Our results further support the concept that ANT can be directly targeted using clinically available 3 T MRI sequences. However, the MRI sequence used by Buentjen's group is 15–20 minutes long and thus requires a guaranteed head stabilization method for the whole scanning time.

Inversion recovery sequences such as STIR improve tissue contrast by suppressing a particular tissue according to the selected inversion time. STIR images with a short inversion time at the point where the difference in longitudinal magnetization between white and gray matter is at its maximum will generate images with a superior contrast between white and gray matter. Together these studies suggest that visualization of ANT is based on the contrast between the gray matter of ANT and enveloping white matter lamina. Importantly, we were also able to demonstrate this white matter–gray matter border with another method using MER.

Our study also has more general implications. Our data clearly demonstrates the weaknesses of indirect AC–PC based targeting. The AC–PC coordinate system was initially used to target structures during the ventriculography era, but it is still used in the current age of CT and MRI for some indications, such as epilepsy. In movement disorder surgery, MRI images are widely used in various degrees to adjust the final target. However, a matter even more important than the technique used in targeting of the structures, is that the AC–PC based coordinate system is still widely used to report the outcome after stereotactic lesions or the postoperative location of DBS electrodes. This most likely causes excessive inconsistencies in the outcome analyses and might, in fact, prevent researchers from identifying the most optimal target. Only very few studies describe the use of "target specific-coordinate

system" in reporting outcome after DBS in movement disorders (Ashkan et al., 2007; Plaha et al., 2006; Vayssiere et al., 2004). Our results also strongly support this concept in ANT-DBS.

In the SANTE-trial (Fisher et al., 2010), DBS lead positions were verified postoperatively with magnetic resonance imaging. The most centrally located contact within each ANT was selected as the active stimulation contact. If no contacts were located inside ANT, the lead was replaced. The stereotactic coordinates used in the study for target definition were provided at a later time. Taking into consideration the information provided by the present study, electrode location assessment with atlas comparisons and MRI sequences not clearly delineating ANT likely contains a factor of uncertainty. Therefore, it is possible that not all of the active contacts in the SANTE-trial were in ANT. The exact knowledge of the location of the electrodes with regard to individual anatomy may lead to increased implantation accuracy and better clinical response. Trial results should also be interpreted accordingly. We intend to explore this matter in further studies.

A finding with significant clinical importance was that the ANT models in our patients in MRI were located more superiorly, laterally and anteriorly compared to the anatomic atlas of Schaltenbrand (Fig. 2). The stereotactic coordinates used in implantation procedures reported in the literature are 12 mm superior, 5–6 mm lateral and 0–2 mm anterior to the mid-commissural point (Schaltenbrand and Wahren, 1998). This point is located at the inferior aspect of the ANT in MRI in majority of our patients. It is important to notice that the success of electrode implantation to the ANT will depend not only on the selected target but also on the selected trajectory to the target point. Indirect targeting of the point above using a transventricular approach results most likely in a penetration of the main part of the ANT. However, if a more lateral transparenchymal approach is selected to avoid penetrating the ventricle, the trajectory may only reach an inferior aspect of the ANT. This may have clinical significance with respect to therapeutic effects.

In the present study, we have used the visualized boundaries of the ANT to study the localization of MER samples relative to ANT. Similar target specific coordinate systems have been described previously to the globus pallidus (Vayssiere et al., 2004) and posterior subthalamic area/caudal zona incerta (Ashkan et al., 2007; Plaha et al., 2006). As the Schaltenbrand atlas is composed of brain slices obtained from three different individuals, efforts have been made to produce atlases

scalable to individual anatomy. The Talairach atlas offers a concept of proportionality, but adapting it to individual brain dimensions makes an assumption that homothetic transformation between two brains is possible, which apparently has not been proven. We are acutely aware of the small number of subjects in our study. However, stereotactic surgery is being performed all over the world using the Schaltenbrand atlas that is based on cadaver samples from only three individuals. (Bajcsy, et al., 1983; Davatzikos, 1996; Vayssiere et al., 2002)

It can be stated that using a coordinate system based on visible landmarks in the MRI that are as close as possible to the area of interest should provide the most accurate results. In our data, for instance distinguishing spikes originating from VA and ANT was possible due to the fact that the visible white matter lamina between these nuclei was used as a landmark of the coordinate system. More distant anatomical landmarks such as AC and PC failed to distinguish these samples.

5. Conclusion

Our data suggest that ANT can be directly visualized using 3 T MRI due to enveloping white matter structures. Anatomical variation in the anterior thalamic area is extensive, and therefore direct visualization is superior to indirect targeting for accurate implantation. Extensive anatomical variation also calls for more detailed analyses of active contact locations in interpreting results from both past and current treatment trials. Further studies with clinical results are needed to prove whether direct targeting also translates to superior seizure control.

Acknowledgements

References

Ashkan, K., Blomstedt, P., Zrinzo, L., Tisch, S., Yousry, T., Limousin-Dowsey, P., Hariz, M.I., 2007. Variability of the subthalamic nucleus: the case for direct MRI guided targeting. Br. J. Neurosurg. 21 (2), 197–200. http://dx.doi.org/10.1080/02688690701272240174453788.

Bajcsy, R., Lieberson, R., Reivich, M., 1983. A computerized system for the elastic matching of deformed radiographic images to idealized atlas images. J Comput Assist Tomogr 7 (4), 618–625. http://dx.doi.org/10.1097/00004728-198308000-000086602820.

Buentjen, L., Kopitzki, K., Schmitt, F.C., Voges, J., Tempelmann, C., Kaufmann, J., Kanowski, M., 2014. Direct targeting of the thalamic anteroventral nucleus for deep brain stimulation by T1-weighted magnetic resonance imaging at 3 T. Stereotact. Funct. Neurosurg. 92 (1), 25–30. http://dx.doi.org/10.1159/00035152524216749.

Child, N.D., Benarroch, E.E., 2013. Anterior nucleus of the thalamus: functional organization and clinical implications. Neurology 81 (21), 1869–1876. http://dx.doi.org/10.1212/01.wnl.0000436078.95856.5624142476.

Davatzikos, C., 1996. Spatial normalization of 3D brain images using deformable models. J Comput Assist Tomogr 20 (4), 656–665. http://dx.doi.org/10.1097/00004728-199607000-000318708076.

Fisher, R., Salanova, V., Witt, T., Worth, R., Henry, T., Gross, R., Oommen, K., Osorio, I., Nazzaro, J., Labar, D., Kaplitt, M., Sperling, M., Sandok, E., Neal, J., Handforth, A., Stern, J., DeSalles, A., Chung, S., Shetter, A., Bergen, D., 2010. Electrical stimulation of the anterior nucleus of thalamus for treatment of refractory epilepsy. Epilepsia 51 (5), 899–908. http://dx.doi.org/10.1111/j.1528-1167.2010.02536.x20331461.

Hodaie, M., Wennberg, R.A., Dostrovsky, J.O., Lozano, A.M., 2002. Chronic anterior thalamus stimulation for intractable epilepsy. Epilepsia 43 (6), 603–608. http://dx.doi.org/10.1046/j.1528-1157.2002.26001.x12060019.

Kerrigan, J.F., Litt, B., Fisher, R.S., Cranstoun, S., French, J.A., Blum, D.E., Dichter, M., Shetter, A., Baltuch, G., Jaggi, J., Krone, S., Brodie, M., Rise, M., Graves, N., 2004. Electrical stimulation of the anterior nucleus of the thalamus for the treatment of intractable epilepsy. Epilepsia 45 (4), 346–354. http://dx.doi.org/10.1111/j.0013-9580.2004.01304.x15030497.

Lee, K.J., Shon, Y.M., Cho, C.B., 2012. Long-term outcome of anterior thalamic nucleus stimulation for intractable epilepsy. Stereotact. Funct. Neurosurg. 90 (6), 379–385. http://dx.doi.org/10.1159/00033999122922474.

Mai, J.K., Paxinos, G., Voss, T., 2007. Atlas of the Human Brain third edition. Academic Press.

Plaha, P., Ben-Shlomo, Y., Patel, N.K., Gill, S.S., 2006. Stimulation of the caudal zona incerta is superior to stimulation of the subthalamic nucleus in improving contralateral Parkinsonism. Brain J. Neurol. 129 (7), 1732–1747. http://dx.doi.org/10.1093/brain/awl12716720681.

Schaltenbrand, G., Wahren, W., 1998. Atlas for Stereotaxy of the Human Brain second edition. Thieme, Stuttgart.

Stypulkowski, P.H., Giftakis, J.E., Billstrom, T.M., 2011. Development of a large animal model for investigation of deep brain stimulation for epilepsy. Stereotact. Funct. Neurosurg. 89 (2), 111–122. http://dx.doi.org/10.1159/00032334321336007.

Van Buren, J.M., Borke, R.C., 1972. The mesial temporal substratum of memory. Anatomical studies in three individuals. Brain J. Neurol. 95 (3), 599–6324655285.

Vayssiere, N., Hemm, S., Cif, L., Picot, M.C., Diakonova, N., El Fertit, H., Frerebeau, P., Coubes, P., 2002. Comparison of atlas- and magnetic resonance imaging-based stereotactic targeting of the globus pallidus internus in the performance of deep brain stimulation for treatment of dystonia. J. Neurosurg. 96 (4), 673–679. http://dx.doi.org/10.3171/jns.2002.96.4.067311990806.

Vayssiere, N., van der Gaag, N., Cif, L., Hemm, S., Verdier, R., Frerebeau, P., Coubes, P., 2004. Deep brain stimulation for dystonia confirming a somatotopic organization in the globus pallidus internus. J. Neurosurg. 101 (2), 181–188. http://dx.doi.org/10.3171/jns.2004.101.2.018115309906.

Yamada, K., Akazawa, K., Yuen, S., Goto, M., Matsushima, S., Takahata, A., Nakagawa, M., Mineura, K., Nishimura, T., 2010. MR imaging of ventral thalamic nuclei. A.J.N.R. Am. J. Neuroradiol. 31 (4), 732–735. http://dx.doi.org/10.3174/ajnr.A187019926703.